SU(4) symmetry breaking and induced superconductivity in graphene quantum Hall edges

Joseph J. Cuozzo and Enrico Rossi
Department of Physics, William & Mary, Williamsburg, Virginia 23187, USA

(Received 13 July 2023; revised 4 June 2024; accepted 9 July 2024; published 25 July 2024)

In graphene, the approximate SU(4) symmetry associated with the spin and valley degrees of freedom in the quantum Hall (QH) regime is reflected in the fourfold degeneracy of graphene's Landau levels (LLs). Interactions and the Zeeman effect break such approximate symmetry and lift the corresponding degeneracy of the LLs. We study how the breaking of the approximate SU(4) symmetry affects the properties of graphene's QH edge modes located in proximity to a superconductor. We show how the lifting of the fourfold degeneracy qualitatively modifies the transport properties of the QH-superconductor heterojunction. For the zero LL, by placing the edge modes in proximity to a superconductor, it is, in principle, possible to realize a 1D topological superconductor supporting Majoranas in the presence of sufficiently strong Zeeman field. We estimate the topological gap of such a topological superconductor and relate it to the properties of the QH-superconductor interface.

DOI: 10.1103/PhysRevB.110.024518

I. INTRODUCTION

Heterojunctions formed by two-dimensional electron gases (2DEGs) in the quantum Hall (QH) regime, placed in the proximity of a superconductor (SC), are ideal to realize one-dimensional topological superconductors [1–4] and are the only realistic systems in which it is expected that not only Majorana zero modes [5] but also more complex non-Abelian anyons can be realized [1,2,6]. In recent years, advances in material and device fabrication have allowed the realization of high-quality QH-SC systems [7–13] that have shown signatures of superconducting correlations induced in the edge modes of QH states. Such experiments have motivated several theoretical works [14–26] that addressed some of the limitations of simple models. QH-SC systems based on graphene [7–11,13] are particularly promising for several reasons: by encapsulating the graphene layer in hexagonal boron nitride (hBN), high-quality, low-disorder devices can be realized; they can be driven into robust QH states with smaller values of the magnetic field (B) than regular 2DEGs due to the fact that for 2D Dirac materials the Landau level (LL) energies E_n scale with the square root of B, $E_n = \mathrm{sgn}(n) v_F \sqrt{2e\hbar B|n|}$ with v_F the graphene's Fermi velocity and $n \in \mathbb{N}$ [27,28], rather than linearly with B, as for 2D systems with parabolic bands. These features have recently enabled the observation of superconducting correlations between the edge states of fractional QH states [11], the first step toward the realization of parafermions.

In any QH-SC system, due to the large magnetic field necessary to drive the 2DEG into the QH regime, the presence of a Zeeman term is unavoidable. Given that almost all known superconductors are spin singlet superconductors, in almost all QH-SC systems the QH edge states that can be paired via the proximity effect are counter-propagating states with opposite spin polarization. As a consequence, our results, by showing how the spin-polarization affects the properties of edge states at QH-SC interfaces, are important to assess the feasibility, even in the ideal conditions of no disorder and extremely low temperatures, of realizing 1D topological superconducting states, supporting non-Abelian quasiparticle states at their ends, using QH-SC systems.

In graphene, due to the spin and valley degeneracy, we have an approximate fourfold degeneracy of the fermionic states. As a consequence, in the presence of a strong perpendicular magnetic field, graphene well approximates a SU(4) quantum Hall Ferromagnet [29–32]. The approximate SU(4) symmetry is broken by Zeeman and interaction effects [33–36]. The breaking of the SU(4) symmetry can significantly affect the strength of the superconducting correlation induced among the QH's edge modes by proximity to a SC, and therefore modify the conditions required for the realization of non-Abelian anyons in QH-SC systems.

In this paper, we study the effect that the breaking of the SU(4) symmetry of graphene's Landau levels (LLs) has on the nature and strength of electron-hole (e-h) conversion processes (Andreev reflection processes) at the interface between the integer QH (IQH) edge and an s-wave superconductor. For $n > 0$ LLs, the breaking of the the SU(4) symmetry causes the edge modes' drift velocity (v_d) to be spin and valley dependent, and we find that this causes the e-h conversion probability, $T_{\text{h-e}}$, to oscillate as function of strength of the SU(4) symmetry breaking terms. For the $E_n = 0$ LL, the Coulomb interaction induces correlated phases [34–44] that lift the degeneracy between particlelike and holelike states and so breaks the effective SU(4) symmetry of the LL, and we find that the interplay of the interaction's effects and Zeeman splitting (Δ_Z) can strongly affect the transport properties of the $E_n = 0$ QH-edge modes at a QH-SC interface. Our results show the effect that SU(4) breaking terms have on the e-h conversion in graphene-based QH-SC systems and how, conversely, signatures in the transport properties of QH-SC edges can be used to estimate the relative strength of such terms. The dependence of such transport properties on Δ_Z can also be used to estimate the efficiency of e-h conversion at QH-SC interfaces.

II. MODEL

We consider the setup shown schematically in Fig. 2(a) in which an interface of length $L_{\rm sc}$ is present between a SC and a graphene layer in the IQH regime. In this situation, the IQH edge modes, along the QH-SC interface, form a chiral Andreev edge state (CAES), a coherent superposition of e-like and h-like edge states [45–49]. For graphene, we assume armchairlike boundaries. Such boundaries do not have intrinsic edge modes, like zigzag edges [50,51], and therefore allow us to better study the intrinsic properties of QH edge states [50]. It is also expected that in most experimental setups, armchairlike boundaries better approximate the devices' edges than zigzag edges.

For $E_n > 0$ LLs, the SU(4) symmetry breaking can be described by taking into account the presence of a Zeeman term of strength Δ_Z that splits the spin degeneracy and a similar term, of strength Δ_v, that lifts the valley degeneracy. We consider an effective low-energy Boguliubov–de Gennes Hamiltonian ($H_{\rm BdG}$) for the one-dimensional (1D) edge modes located at the interface between the QH systems and the SC. Assuming that no magnetic field is present in the SC, we have

$$\hat{H}_{\rm BdG} = \psi^\dagger[\hbar v_d k \tau_0\eta_0\sigma_0 - \hbar v_d k_F \tau_z\eta_0\sigma_0 + (\Delta_Z/2)\tau_0\eta_0\sigma_z + \hat{\Delta}_{K_1K_2} + \Delta\tau_x\eta_0\sigma_0]\psi, \quad (1)$$

where $\psi = (c_{kK_1\uparrow}, c_{kK_1\downarrow}, c_{kK_2\uparrow}, c_{kK_2\downarrow}, c^\dagger_{-kK_2\downarrow}, -c^\dagger_{-kK_2\uparrow}, c^\dagger_{-kK_1\downarrow}, -c^\dagger_{-kK_1\uparrow})^T$, with $c^\dagger_{kK_i\sigma}$, $c_{kK_i\sigma}$ the creation and annihilation operators, respectively, for an electron with momentum k, and spin $\sigma = \uparrow, \downarrow$, in the K_i valley. $\epsilon_k = \hbar v_d k$ is the edge mode's dispersion along the QH-SC interface with v_d the drift velocity, τ_i, η_i, and σ_i are 2×2 Pauli matrices in particle-hole, valley, and spin space, respectively, Δ is the mean-field superconducting gap, and k_F is the Fermi wave vector at the Fermi energy E_F. In Eq. (1), $\hat{\Delta}_{K_1K_2} = \Delta_v/2[\cos(\theta_v)\tau_0\eta_z\sigma_0 + \sin(\theta_v)\cos(\phi)\tau_z\eta_x\sigma_0 + \sin(\theta_v)\sin(\phi)\tau_z\eta_y\sigma_0]$, where θ_v, ϕ are the angles that parametrize the direction in valley space of the mean field lifting the valley degeneracy. For $E_n > 0$ LLs, SU(4) breaking terms affect the transport properties of the QH-SC edge by causing the edge modes' drift velocity v_d to be spin and valley dependent. This is due to two mechanisms: (i) such terms cause the effective tunneling between the QH region and the SC to be dependent on the SU(4) flavor (see Appendix B and (ii) the splitting due to these terms causes edge states of different SU(4) flavors to have different Fermi wave vectors and, therefore, when the confining potential $V(y)$ is not linear, different drift velocities. To exemplify the physics, below we consider in detail the second mechanism given that the further inclusion of the first mechanism is straightforward and its effect is also in general quite smaller (see Appendix B).

To understand how Δ_Z induces a spin-dependent v_d, we can consider the simple case when $V(y) = V_0 y^2/(l_V)^2$ for $y > 0$ and $V(y) = 0$ for $y < 0$. V_0 and l_V are constants that characterize the confining potential. Considering that $y = l_B^2 k$, with l_B the magnetic length, in the limit $dV/dy|_{\epsilon_k=0} \ll \hbar\omega_c/l_B$, where ω_c is the cyclotron frequency, we obtain $v_{d\uparrow\downarrow} = v_d[\tilde{\epsilon}_F \mp \Delta_Z/2]^{1/2}$, with $v_d = 2[l_B^2/(\hbar l_V)][V_0\tilde{\epsilon}_F]^{1/2}$, and $\tilde{\epsilon} \equiv E_F - E_n$, E_F being the Fermi energy; see Fig. 1(b) and Appendix A. In the limit $\Delta_Z \ll 2\tilde{\epsilon}_F$, we have $v_{d\uparrow\downarrow} = v_d[1 \pm \Delta_Z/(4\tilde{\epsilon}_F)]$.

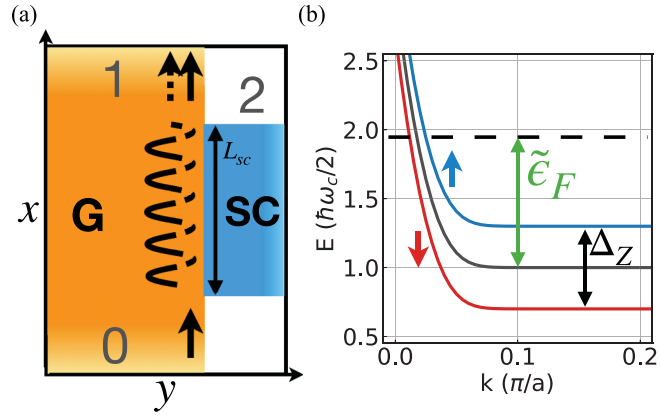

FIG. 1. (a) Schematic of the QH-SC setup. (b) Dispersion of LL with Zeeman splitting.

We first consider the case when $\Delta_Z \neq 0$ and $\Delta_v = 0$. This situation is also directly relevant to QH-SC heterostructures based on standard 2DEG systems. In this case $H_{\rm BdG}$ can be block-diagonalized with blocks $\hat{H}_\pm = \psi^\dagger_\pm H_\pm \psi_\pm$, where $H_\pm$ are 2×2 matrices and $\psi_+ = (c_{k\uparrow}, c^\dagger_{-k\downarrow})$, $\psi_- = (c_{k\downarrow}, -c^\dagger_{-k\uparrow})$. Here we drop the valley indices since in this case the valleys are degenerate. From the expressions of $H_\pm$ and the BdG equation $H_\pm\Phi_\pm(x) = E\Phi_\pm(x)$, we can calculate the transfer matrices [48,52]

$$M_\pm(L,\,0) = e^{i\alpha}\begin{pmatrix} t_\pm & \mp i a_\pm \\ \mp i a_\pm & t^*_\pm \end{pmatrix} \quad (2)$$

that relate the CAES's state at the end, $x = L_{\rm sc}$, of the QH-SC interface, to the CAES's state at the beginning, $x = 0$, of the interface. In Eq. (2), α is a trivial phase and $a_\pm$ describes the mixing of electrons and holes along the interface. Knowing $M_\pm$, we can obtain the probability for Andreev conversion $T^{(\pm)}_{\rm h\text{-}e} = |a_\pm|^2$ of an electron with spin $+/- = \uparrow, \downarrow$ from lead 0 to lead 1 [see Fig. 1(a)]:

$$T^{(\pm)}_{\rm h\text{-}e} = \frac{\Delta^2 \sin^2(L_{\rm sc}\delta k_{\rm e0h,\pm})}{(\hbar v_s\,\delta k_{F,\pm})^2}, \quad (3)$$

with

$$\delta k_{\rm h\text{-}e\pm} = \frac{1}{\hbar v_s}\sqrt{\Delta^2 + \left(\frac{\hbar v_s k_F \pm \hat{v}E - \hat{v}\Delta_Z/2}{1-\hat{v}^2}\right)^2}. \quad (4)$$

In Eqs. (3) and (4), $\hat{v} \equiv v_a/v_s$, with $v_s \equiv (v_{d\uparrow} + v_{d\downarrow})/2$, $v_a \equiv (v_{d\uparrow} - v_{d\downarrow})/2$.

The knowledge of $T^{(\pm)}_{\rm h\text{-}e}$ allows us to obtain the resistance R_D between the superconducting terminal 2 and terminal 1 in the absence of backscattering [10–12,21]. For filling factor ν, we have

$$R_D = \frac{R_H}{\nu}\frac{(\nu - 2T_{\rm h\text{-}e})}{2T_{he}} \quad (5)$$

where $R_H = h/e^2$. For our case, $\nu = 6$ (including the $E_n = 0$ LLs) and $T_{\rm h\text{-}e} = 2(T^{(+)}_{\rm h\text{-}e} + T^{(-)}_{\rm h\text{-}e}) + 2T^{(0)}_{\rm h\text{-}e}$ and $T^{(0)}_{\rm h\text{-}e} = T^{(+)}_{\rm h\text{-}e}(E = 0, v_a = 0, \Delta_{v/Z} = 0)$ describes the Andreev conversion of $n = 0$ LL states for which asymmetries due to

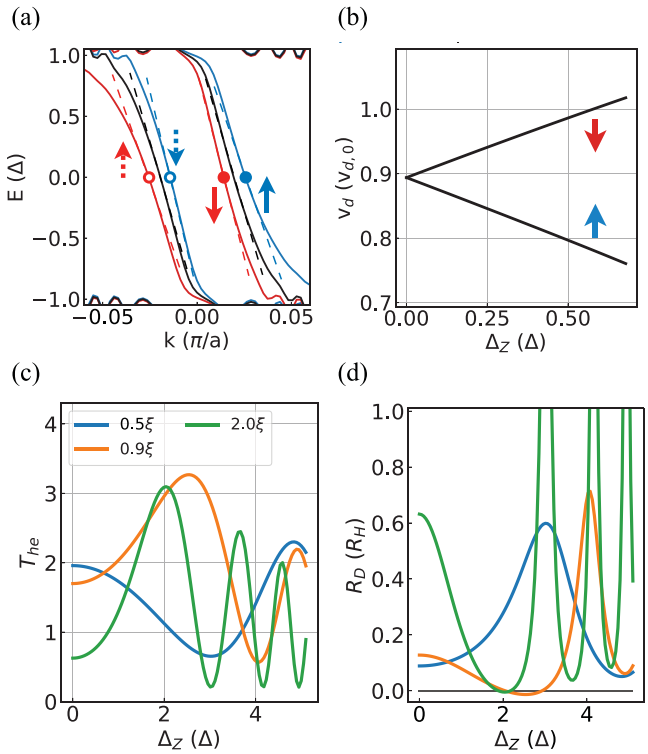

FIG. 2. (a) BdG spectrum of a hybrid QH-SC structure in the LL with and without (black) Zeeman field. (b) Drift velocity of CAESs normalized by the vacuum drift velocity versus the Zeeman field. $T_{\text{h-e}}$ (c), and R_D (d), for $\tilde{\epsilon}_F = 10\,\Delta$, $v_s = 0.1\Delta\xi/\hbar$, $k_F = 5\hbar/\xi$, and $L_{\text{sc}} = (0.5, 0.9, 2.0)\xi$.

splittings are negligible. Equations (3)–(5) show how the spin dependence of the edge mode velocities, by modifying $\delta k_{\text{h-e}}$, affects the electron-hole conversion taking place along the QH-SC interface and its transport properties.

III. EFFECTS OF ZEEMAN AND VALLEY SPLITTING

To obtain a quantitative estimate of the effect of SU(4)-breaking terms, we have also obtained the transport properties at the QH-SC interface using a tight-binding (TB) model implemented via the KWANT package [53]. Details of the model can be found in Appendix C. Figure 2(a) shows the dispersion of the CAES when $E_n > 0$ both for the case when $\Delta_Z{=}\Delta_v{=}0$, and the one for which $\Delta_v = 0$ but $\Delta_Z \neq 0$. Figure 2(b) shows the effect of Δ_Z on the renormalized, spin-dependent drift velocity. In the limit $\Delta_Z = 0$, for the chosen parameter values, tunneling processes into the SC cause the renormalized v_d to be $\sim 9/10$ of the v_d at a QH-vacuum interface. The results of Fig. 2(b) show that the scaling $v_{d\sigma} \propto \sigma\,\Delta_Z$, for $\Delta_Z \ll \tilde{\epsilon}_F$, obtained assuming a quadratic edge potential agrees well with the scaling obtained from the TB-model calculation for Δ_Z as large as $\sim 0.5\tilde{\epsilon}_F$ Figures 2(c) and 2(d) show the total e-h conversion probability, $T_{\text{h-e}}$, and R_D as a function of Δ_Z for $\nu = 6$ and various L_{sc}, obtained assuming for $v_\uparrow(\Delta_Z)$ and $v_\downarrow(\Delta_Z)$ the scalings $\pm\Delta_Z/(2\tilde{\epsilon}_F)$ consistent with Fig. 2(b). In the limit of $L_{\text{sc}} > \xi$, Fig. 2(d), we find that $T_{\text{h-e}}$ oscillates with Δ_Z and that the period of the oscillations decreases with Δ_Z, in accordance with Eq. (4).

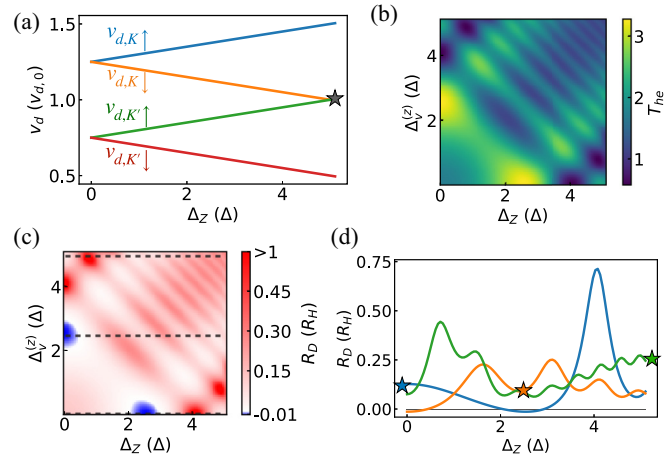

FIG. 3. (a) Drift velocities versus Δ_Z for $\theta_v = 0$, $\Delta_v = \tilde{\epsilon}_F/2$, and $\tilde{\epsilon}_F = 10\,\Delta$. (b) $T_{\text{h-e}}$ versus Δ_Z and Δ_v for $L_{\text{sc}} = 0.9\,\xi$, $v_{s,s} = 0.1\Delta\xi/\hbar$, and $k_F = 5\hbar/\xi$. (c) R_D corresponding to (b). (d) Line cuts of R_D for fixed $\Delta_v = (0, 2.5, 5)\Delta$, blue, orange, and green traces, respectively. Stars denote the values of R_D when $\Delta_Z = \Delta_v$.

The results shown in Figs. 2(c) and 2(d) are qualitatively valid also when the term $\hat{\Delta}_{K_1K_2}$ does not break time reversal (TR) symmetry, i.e., when $\theta_v = \pi/2$, considering that the TR operator in valley space is $\Theta_v = \mathcal{C}\eta_x$, with $\mathcal{C}$ denoting complex conjugation. As a consequence, for $\theta_v = \pi/2$, $\hat{\Delta}_{K_1K_2}$ only affects the average value of the drift velocity and does not induce an asymmetry between the drift velocities of the e-like and h-like states. The resulting transport properties at the QH-SC edge mode are obtained from Eqs. (3)–(5) by simply taking into account the renormalization of v_s due to $\hat{\Delta}_{K_1K_2}$.

When $\theta_v \neq \pi/2$, the term $\hat{\Delta}_{K_1K_2}$ breaks TR symmetry and causes the drift velocities of the time-reversed edge modes to be different. In this case, the effect of $\hat{\Delta}_{K_1K_2}$ can compound, or compensate, the effect of Δ_Z. Let $v_{s,K_i} \equiv (v_{d\uparrow K_i} + v_{d\downarrow K_i})/2$, $v_{a,K_i} \equiv (v_{d\uparrow K_i} - v_{d\downarrow K_i})/2$, and $v_{s,s} \equiv (v_{s,K_1} + v_{s,K_2})/2$, $v_{s,a} \equiv (v_{s,K_1} - v_{s,K_2})/2$, $v_{a,s} \equiv (v_{a,K_1} + v_{a,K_2})/2$, $v_{a,a} \equiv (v_{a,K_1} - v_{a,K_2})/2$. Using these definitions, and setting without loss of generality $\phi = 0$, for the case when $\theta_v = 0$, the BdG Hamiltonian, including the valley degrees of freedom, takes the form

$$\begin{aligned}\hat{H}_{\text{BdG}} = \psi^\dagger[&\hbar v_{s,s}k\tau_0\eta_0\sigma_0 + \hbar v_{s,a}k\tau_z\eta_z\sigma_0 + \hbar v_{a,s}k\tau_z\eta_0\sigma_z \\ &+ \hbar v_{a,a}k\tau_0\eta_z\sigma_z + (\Delta_Z/2)\tau_0\eta_0\sigma_z + (\Delta_v/2)\tau_0\eta_z\sigma_z \\ &- \hbar v_{s,s}k_F\tau_z\eta_0\sigma_0 + \Delta\tau_x\eta_0\sigma_0]\psi. \end{aligned} \tag{6}$$

Figure 3(a) shows the drift velocities v_{σ,K_i} as a function of Zeeman splitting for $\theta_v = 0$ and fixed Δ_v obtained assuming a quadratic edge potential and $\Delta_{v,Z} \leqslant \tilde{\epsilon}_F/2$. From the values v_{σ,K_i}, we can block diagonalize Eq. (6) and calculate the momentum difference between coupled electron and hole modes. Then we use Eqs. (3) and (5) to obtain $T_{\text{h-e}}$ and R_D. We see that as Δ_Z increases, the velocity asymmetry becomes larger for a pair of CAESs while becoming smaller for the other pair until it vanishes when $\Delta_Z = \Delta_v$. One could expect a maximum $T_{\text{h-e}}$ at this point, but Fig. 3(b) shows that while a mirror symmetry about the $\Delta_Z = \Delta_v$ line exists, $T_{\text{h-e}}$ is not maximum along this line. Figure 3(c) shows the dependence of R_D on Δ_Z and Δ_v.

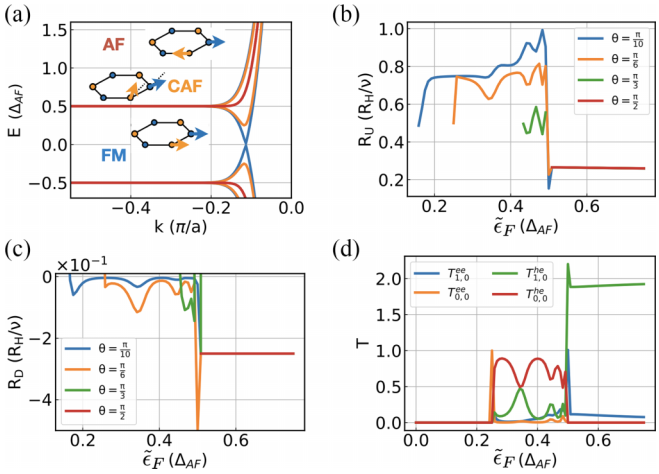

FIG. 4. (a) Dispersion of $E_n = 0$ graphene LL for the FM, CAF, and AF phases with schematics illustrating the canting of spins on different sublattices for each phase. R_U (b), and R_D (c), as a function of $\tilde{\epsilon}_F$ in the CAF phase. (d) $T^{\text{e-e}}_{j,i}$ and $T^{\text{h-e}}_{j,i}$ versus $\tilde{\epsilon}_F$ for $\theta = \pi/6$. $L_{sc} = 0.675\xi$.

We find that when $\theta_v = 0$, the dependence of R_D on Δ_Z is different depending on the value of Δ_v, as shown by the line cuts presented in Fig. 3(d): the period of the oscillations of R_D with respect to Δ_Z decreases as Δ_v increases. By comparing the experimentally measured R_D as a function of Δ_Z, by tuning the in-plane component of the magnetic field, results like the ones in Fig. 3(d) could allow the estimation of the strength of the valley splitting term breaking time-reversal symmetry.

IV. $n = 0$: CANTED ANTIFERROMAGNETIC STATE

In the $E_n = 0$ LL, we have a degeneracy between particlelike and holelike states. However, for the $E_n = 0$ LL, we also have that the valley and sublattice degree of freedom are locked to each other. Taking into account the spin degree of freedom, the full, approximate symmetry for the $E_n = 0$ LL is still SU(4). Besides the Zeeman effect, such approximate symmetry is broken by interaction effects that drive the system into a correlated state. Theoretical [37,39] and experimental results [36,38,40,41,44] have shown that the likely correlated state is a canted antiferromagnetic (CAF) state in which the spin degree of freedom is locked with the sublattice degree of freedom as shown schematically in the inset of Fig. 4(a). Recent measurements [42,43], however, have shown evidence for the establishment of an intervalley coherent phase characterized by a Kekulé distortion [54]. Recent theoretical works [55,56] have shown that the CAF and Kekulé phases can coexist. Such coexistence would reconcile the recent observations and the previous ones suggesting the presence of a CAF phase. For Δ_Z much smaller than the interaction strength U_{int}, also for $E_n = 0$ LL, both in the CAF and Kekulé phase, the effect of Δ_Z on the transport properties at the QH-SC interface is described by Eqs. (2)–(5). When Δ_Z is comparable to or larger than U_{int}, its effect on the transport properties of the QH-SC interface can be significantly different from the one described by Eqs. (2)–(5) [57], but qualitatively the same in the Kekulé phase and CAF phase. In the remainder we focus on the CAF phase.

For $\Delta_Z \ll U_{\text{int}}$, the CAF phase corresponds to an antiferromagnetic (AFM) state, whereas for $\Delta_Z \gg U_{\text{int}}$ the CAF phase describes a ferromagnetic (FM) state [38]; see inset Fig. 4(a). To describe the CAF phase to the tight-binding Hamiltonian for graphene (section IV of the SM), we add the term $H_{\text{AFM}} = (\Delta_{\text{AFM}}/2)[\sum_i (\psi^\dagger_{A_i} \tau_z \sigma_x \psi_{A_i} - \psi^\dagger_{B_i} \tau_z \sigma_x \psi_{B_i})]$, where $\psi^\dagger_{S_i}$, ψ_{S_i}, are the creation and annihilation operators for an electron at site $S_i = (A_i, B_i)$ with A_i, B_i the sites of sublattices A, B, respectively, and Δ_{AFM} the strength of the mean-field describing the AFM phase. The term H_{AFM}, without Zeeman splitting, induces a bulk and edge gap at the charge neutrality point, as seen in Fig. 4(a).

To describe the evolution from the AFM phase to the FM phase, we set $\Delta_{\text{AFM}} = \Delta_0 \sin\theta$ and $\Delta_Z = \Delta_0 \cos\theta$, where $\Delta_0 \equiv [\Delta^2_{\text{AFM}} + \Delta^2_Z]^{1/2}$ is the total magnitude of the bulk gap, and 2θ is the angle between the spin projections on sublattices A and B. Figure 4(a) shows the evolution of the LL close to the neutrality point as θ is varied: Gor $\theta = 0$, we recover the FM phase, and for $\theta = \pi/2$ the AFM phase. When $\Delta_Z \neq 0$, the lowest energy particlelike and holelike states approach close to the edge causing the gap between edge states (Δ_{edge}) to be smaller than the gap between bulk states; Fig. 4(a). For $\Delta_Z \neq 0$, close to the edge, the spin polarization becomes momentum dependent so forward and backward moving modes have opposite spin polarizations. As a consequence, when $\Delta_Z \sim \Delta_{\text{AFM}}$, for the QH edge in proximity of the SC we can have strong Andreev retroreflection.

Figures 4(b) and 4(c) show the calculated resistance R_U between terminal 2 and 0, and R_D, respectively, as a function of $\tilde{\epsilon}_F$ for the $E_n = 0$ LL in the CAF phase for different values of θ. Given that for $\Delta_Z \gtrsim \Delta_{\text{AFM}}$ we can have counterpropagating modes, the equations for R_D, Eq. (5), and R_U have to be generalized to take into account backscattering processes; see Fig. 4(d) and SM. As θ increases R_U decreases. This fact could be used to extract the effect of interactions on the dispersion of the $E_n = 0$ LL's edge modes.

For $\Delta_Z \gtrsim \Delta_{\text{AFM}}$, as we approach the FM phase, the $n = 0$ LL has counterpropagating edge modes with nontrivial spin structure that appear to be ideal for the realization of a 1D topological superconducting state supporting Majoranas at its ends [4]. However, using realistic parameter values and the full graphene-SC TB model, we find that no Majoranas are present. To understand the issue, we map the CAF edge states to the effective 1D model $H = t\hat{k}^2 - \epsilon_F + \alpha\hat{k}\sigma_y + J_Z\sigma_z$ with $\hat{k} \equiv ak$, $a = 2.46$ Å being graphene's lattice constant, and extract t and α from fitting the LL's edges dispersion obtained from the tight-binding model; see Fig. 7. For $\theta = \pi/4$, using the TB model parameters presented in Appendix D, we find $t = 63\Delta$, $\alpha = 7\Delta$. Given that for the CAF regime considered we only have one helical band, we can set $\epsilon_F = 0$ and set J_Z equal to the chemical potential of the single helical band. In the remainder, we set $J_Z = 4\Delta$. The key difference between the ideal 1D model and the edge at the QH-SC interface is that for the latter the minimum of the bands when $\alpha = 0$, in general, is not located at a time-reversal invariant momentum ($k = 0$), that for a QH-SC system corresponds to the edge between QH region and SC. To take this into account in the

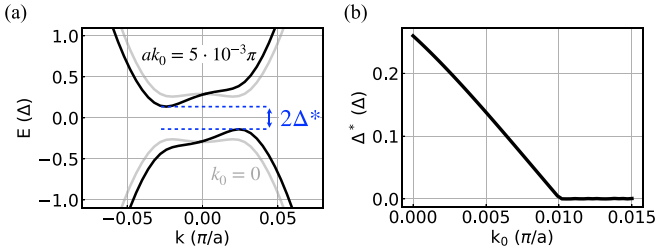

FIG. 5. (a) Spectrum for effective 1D model with finite superconducting pairing Δ and small offset k_0. (b) Topological gap Δ^* as a function of k_0 for a fit corresponding to $\theta = \pi/4$.

effective 1D model, we introduce a momentum offset $k \to k + k_0$. As k_0 increases, the band gap Δ^* induced by the superconducting paring becomes more indirect and is reduced, as can be seen in Fig. 5. We see that Δ^* vanishes when $k_0 \approx 10^{-2}\pi/a$. Considering that for $B = 2\,\mathrm{T}$ $l_B \approx 18$ nm, we have that Δ^* will be vanishing when the distance between QH edge modes and the SC edge is larger than $10^{-2}(\pi/a)l_B^2 \approx 2.3 l_B$. The fact that for realistic parameters' values $k_0 > 10^{-2}\pi/a$ (see Fig. 7) explains why in our TB calculations no Majoranas are observed, and points to an aspect that must be taken into account in experiments.

V. CONCLUSION

In summary, we have studied how the breaking of the approximate SU(4) symmetry of graphene's Landau levels affects the Andreev conversion processes of QH edges states located in proximity of a superconductor. We have found that contrary to statements in previous works, the Zeeman splitting affects the electron-hole conversion probability at QH-SC interfaces. We have shown that this is due to the fact that a Zeeman splitting causes the drift velocity of electron and holes to be spin dependent. In addition, we have included the effect of valley splitting for graphene-based QH-SC heterostructures, shown that it also affects the e-h conversion, and found how such conversion is modified by the interplay of Zeeman and valley splittings. Our results show that, in general, the probability of an electron to be converted into a hole while traveling along the QH-SC interface, due to Andreev processes, can strongly oscillate as a function of the strength of the terms breaking the SU(4) symmetry, inducing oscillations of directly measurable transport properties that could be used to extract the efficiency of the electron-hole conversion and the magnitude of the SU(4) breaking terms. For the $n = 0$ graphene Landau level, we have obtained how three-terminal QH-SC transport properties depend on the Fermi energy for the various SU(4)-symmetry broken canted-antiferromagnetic phases, and on the canting angle of such phases. These results show that the canting angle of a CAF phase of the $n = 0$ graphene's Landau level could be estimated by measuring the transport properties at the QH-SC interface. In the limit of large Zeeman splitting, the edge modes of the $n = 0$ LL have all the properties to allow the realization, when proximitized by a SC, of 1D topological superconducting states with Majoranas. We have shown how the topological gap of such states could be much lower than naïvely expected due to the nature of the edge modes' dispersion at the QH-SC interface. Our results are directly relevant to the ongoing effort to induce superconducting pairing correlations in graphene QH edge states with the ultimate goal to realize non-Abelian anyons.

ACKNOWLEDGMENTS

The work was primarily supported by the U.S. Department of Energy (DOE), Office of Science, Basic Energy Sciences (BES), under Award No. DE-SC0022245. The early stages of this work (through end of 2022) were supported by the Army Research Office under Award No. W911NF-18-1-0290. E.R. also thanks the Aspen Center for Physics, which is supported by NSF Grant No. PHY-1607611, where part of this work was performed, and U. Zülicke and Y. Barlas for helpful discussions.

APPENDIX A: FLAVOR-DEPENDENT DRIFT VELOCITY DUE TO NON-LINEAR CONFINING POTENTIAL

Let us consider the generic Hamiltonian describing a free-electron gas in the two-dimensional (2D) (x, y) plane,

$$H = \hat{\epsilon}(k_x, k_y) + V(y)\mathbb{1} - E_F\mathbb{1}, \tag{A1}$$

where $\hat{\epsilon}(k_x, k_y)$ is a matrix, in orbital space, describing the dispersion of the 2D electron system, $\mathbf{k} = (k_x, k_y)$ is the 2D wave vector, $V(y)$ is the confining potential defining the edge of the sample, and E_F is the Fermi energy. Let us assume that translational symmetry is preserved along the x direction. In this case, to include the effect of a magnetic field B perpendicular to the 2D electron system it is convenient to use the gauge $\mathbf{A} = (-By, 0, 0)$. By replacing in (A1) $\mathbf{k} = (k_x, k_y)$ with $\mathbf{k} - (e/c)\mathbf{A}$, we obtain the energy spectrum

$$E(k) = E_n + V\left(kl_B^2\right) - E_F, \tag{A2}$$

where $\{E_n\}$ are the energies of the Landau levels, $k \equiv k_x$, and $l_B = [\hbar c/(eB)]^{1/2}$ is the magnetic length. Equation (A2) is valid for the common situation when $\partial_y V(y) \ll (E_{n+1} - E_n)/l_B$. $\{E_n\}$ are momentum independent and so the drift velocity of an edge state in the nth Landau level is determined by the confining potential,

$$v_d = \frac{1}{\hbar}\frac{dE_n}{dk} = \frac{1}{\hbar}\frac{dV}{dk}\bigg|_{k_F} = \frac{l_B^2}{\hbar}\frac{dV}{dy}\bigg|_{y_F}, \tag{A3}$$

where k_F is the Fermi wave vector $[E(k_F) = 0]$ and $y_F = k_F l_B^2$. A very natural and physical approximation for the confining potential $V(y)$ is

$$V(y) = \begin{cases} \left(V_0/l_V^2\right)(y - L_0)^2, & y \geqslant L_0 \\ \left(V_0/l_V^2\right)(y + L_0)^2, & y \leqslant -L_0 \\ 0, & -L_0 < y < L_0, \end{cases} \tag{A4}$$

where V_0 (with units of energy) l_V (with units of length) are constants that parametrize the dependence of V on the position, and $2L_0$ is the width of the QH system. For the states at the Fermi energy on the $y > 0$ side of the sample, we have

$$y_F = L_0 + l_V\sqrt{\frac{\tilde{\epsilon}_F}{V_0}}, \tag{A5}$$

where $\tilde{\epsilon}_F \equiv E_F - E_n$, so

$$v_d = \frac{l_B^2}{\hbar}\frac{dV}{dy}\bigg|_{y_F} = \frac{2l_B^2}{\hbar l_V}\sqrt{V_0\tilde{\epsilon}_F}. \tag{A6}$$

In the presence of a Zeeman term, we have the spin degeneracy of the energy levels, $E(k)$ is lifted, and we have $E(k) = E_n + V(kl_B^2) - E_F \pm \Delta_Z/2$ and therefore two different Fermi wave vectors, one for the spin-up state (k_{F+}) and one of the spin-down state (k_{F-}), and, correspondingly, two different values of y_F:

$$y_{F,\pm} = L_0 + l_V\sqrt{\frac{\tilde{\epsilon}_F \mp \Delta_Z/2}{V_0}}. \tag{A7}$$

The fact that $y_{F,+} \neq y_{F,-}$ implies that when $V(y)$ is not linear, the spin-up and spin-down state will have different drift velocities:

$$\begin{aligned} v_{d\uparrow\downarrow} &= \frac{2l_B^2}{\hbar l_V}\sqrt{V_0(\tilde{\epsilon}_F \mp \Delta_Z/2)} \\ &\approx v_d\left(1 \mp \frac{\Delta_Z}{4(\tilde{\epsilon}_F)}\right) = v_d \mp v_a, \end{aligned} \tag{A8}$$

where the approximate expression is valid when $\Delta_Z \ll 2\tilde{\epsilon}_F$, and the–,+ signs apply to the spin $\uparrow$ and $\downarrow$ states, respectively. Thus, the Zeeman effect in combination with a nonlinear confining potential results in a nonzero difference v_a between $v_{d\uparrow}$, and $v_{d\downarrow}$. For the case when a term is present that lifts graphene's valley degeneracy, the same equation (A8) is obtained if such a term also breaks time-reversal symmetry. In this case, Δ_Z should be replaced by Δ_v, the strength of the valley-splitting term.

APPENDIX B: FLAVOR-DEPENDENT DRIFT VELOCITY DUE TO SPIN-DEPENDENT QH-SC TUNNELING STRENGTH

Consider a chiral edge state in the lowest Landau level propagating in the x direction. The low-energy BdG description of a spinful Landau level is

$$\begin{aligned} H_{\rm QH} &= \frac{1}{2}\sum_k \Psi_k^\dagger(v_d k\,\mathbb{1} - E_F\tau_z\sigma_0)\Psi_k \\ &= \frac{1}{2}\sum_k \Psi_k^\dagger\, h_{\rm QH}(\vec{k})\,\Psi_k, \end{aligned} \tag{B1}$$

where v_d is the drift velocity, $\Psi_k^\dagger = (c_{k\uparrow}^\dagger,\, c_{k\downarrow}^\dagger,\, c_{-k\uparrow},\, c_{-k\downarrow})$ is the BdG spinor, and τ_i and σ_i are Pauli matrices in Nambu and spin space, respectively. We take the units where $\hbar = 1$. Suppose we couple this system to an s-wave spin-singlet superconductor described by

$$\begin{aligned} H_{\rm sc} &= \frac{1}{2}\sum_{\mathbf{k}} \Phi_{\mathbf{k}}^\dagger[\xi_{\mathbf{k}}\tau_z\sigma_0 - \Delta\tau_y\sigma_y]\Phi_{\mathbf{k}} \\ &= \frac{1}{2}\sum_{\mathbf{k}} \Phi_{\mathbf{k}}^\dagger\, h_{\rm sc}(\mathbf{k})\,\Phi_{\mathbf{k}}, \end{aligned} \tag{B2}$$

where Δ is the superconducting gap (assumed to be real for simplicity), $\xi_{\mathbf{k}} = \frac{k^2}{2m} - E_{F,s}$, and $\Phi_{\mathbf{k}}^\dagger = (d_{\mathbf{k}\uparrow}^\dagger,\, d_{\mathbf{k}\downarrow}^\dagger,\, d_{-\mathbf{k}\uparrow},\, d_{-\mathbf{k}\downarrow})$. We will describe the coupling between the two systems within the tunneling Hamiltonian description with

$$\begin{aligned} H_T &= \frac{1}{2}\sum_{\mathbf{k}} \Phi_{\mathbf{k}}^\dagger(t_0\tau_z\sigma_0)\Psi_k + \text{H.c.} \\ &= \frac{1}{2}\sum_{\mathbf{k}} \Phi_{\mathbf{k}}^\dagger\, h_T\,\Psi_k + \text{H.c.}, \end{aligned} \tag{B3}$$

where t_0 is the tunneling amplitude associated with electron scattering from the quantum Hall sample to the superconductor and vice versa. The bare Green's function for the superconductor at $T = 0$ is

$$G_{sc}(\mathbf{k},\,\omega) = (\omega - h_{\rm sc}(\mathbf{k}))^{-1} \tag{B4}$$

$$= \frac{\omega\,\mathbb{1} + \xi_{\mathbf{k}}\tau_z\sigma_0 - \Delta\tau_y\sigma_y}{\omega^2 - \xi_{\mathbf{k}}^2 - \Delta^2}. \tag{B5}$$

The self-energy is given by

$$\begin{aligned} \Sigma(\mathbf{k},\,\omega) &= \int d\mathbf{q}\, h_T(\mathbf{q})G_{\rm sc}(\mathbf{k}+\mathbf{q},\,\omega)h_T(-\mathbf{q}) \\ &\approx -\lambda\frac{\omega\,\mathbb{1} + \Delta\tau_y\sigma_y}{\sqrt{\Delta^2 - \omega^2}}, \end{aligned} \tag{B6}$$

where $\lambda = -\pi t_0^2 N_{\rm int}(0)$ and $N_{\rm int}(0)$ is the interface DOS at the Fermi energy. In the limit $\omega \ll \Delta$ from the equation for the poles of the dressed Green's function,

$$\text{Det}(h_{\rm QH}(\mathbf{k}) + \Sigma(\mathbf{k},\,\omega) - \omega) = 0, \tag{B7}$$

we can obtain the effective Hamiltonian [24,58]:

$$H_{\rm eff}(k) = \frac{v_d}{1+\lambda/\Delta}k\,\mathbb{1} - \frac{E_F}{1+\lambda/\Delta}\tau_z\sigma_0 - \frac{\Delta}{1+\Delta/\lambda}\tau_y\sigma_y. \tag{B8}$$

Now we will consider a perturbation to the tunneling Hamiltonian. Consider the Hamiltonian for a vacuum edge state with Zeeman splitting Δ_Z:

$$\begin{aligned} H'_{\rm QH} &= \frac{1}{2}\sum_k \Psi_k^\dagger\left(v_d k\,\mathbb{1} - E_F\tau_z\sigma_0 + \frac{\Delta_Z}{2}\tau_z\sigma_z\right)\Psi_k \\ &= \frac{1}{2}\sum_k \Psi_k^\dagger h'_{\rm QH}(k)\Psi_k. \end{aligned} \tag{B9}$$

Besides the Zeeman effect lifting the degeneracy of the Landau levels, the splitting also spatially separates spin-polarized edge states with opposite spins [59]. This separation occurs in the direction perpendicular to the boundary (y direction in this case). Thus, in a QH/SC heterostructure in the LL, one edge state moves closer to the interface and the other moves further away. To account for this spatial shift, we consider the modified tunneling Hamiltonian,

$$H'_T = \frac{1}{2}\sum_{\vec{k}} \Phi_{\mathbf{k}}^\dagger(t_0\tau_z\sigma_0 + \delta t(\Delta_Z)\,\tau_z\sigma_z)\Psi_k + \text{H.c.}, \tag{B10}$$

where $\delta t = \delta t(\Delta_Z)$ is an odd function in Δ_Z. Now we proceed as before, where we solve for the interface self-energy with the modified tunneling Hamiltonian. Doing this,

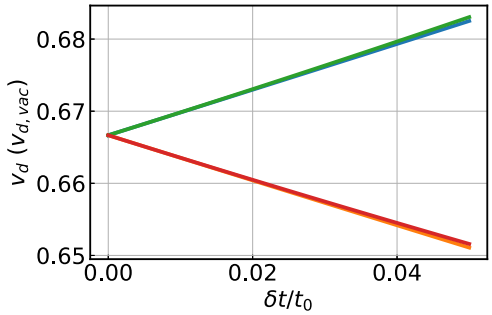

FIG. 6. Drift velocity of edge states as a function of δt for $E_F = \Delta/2$, $\lambda = \Delta/2$, $\Delta_Z = 0$, and $v_d = 5 \times 10^2 a\Delta$.

we find

$$\Sigma'(\mathbf{k},\,\omega) = \int d\mathbf{q}\, h'_T(\mathbf{q}) G_{\rm sc}(\mathbf{k}+\mathbf{q},\,\omega) h'_T(-\mathbf{q}) \tag{B11}$$

$$\approx \Sigma(\mathbf{k},\,\omega) - 2\lambda \frac{\delta t}{t_0}\left(\frac{\omega\tau_0\sigma_z}{\sqrt{\Delta^2-\omega^2}}\right) + \mathcal{O}((\delta t/t_0)^2). \tag{B12}$$

Then the energy eigenvalues describing the Andreev edge states are determined by the BdG equationL

$$\mathrm{Det}(h'_{\rm QH}(k) + \Sigma'(\omega) - \omega) = 0. \tag{B13}$$

Assuming the low-energy case $\omega \ll \Delta$, we have

$$\mathrm{Det}\Bigg[v_d k \mathbb{1} - E_F \tau_z\sigma_0 - \lambda\tau_y\sigma_y + \frac{\Delta_Z}{2}\tau_z\sigma_z - \tau_0\left(\sigma_0 + \frac{\lambda}{\Delta}\left(1 + 2\frac{\delta t}{t_0}\sigma_z\right)\right)\omega\Bigg] \approx 0. \tag{B14}$$

The matrix structure of the equation does not allow one to easily extract an effective Hamiltonian description. The equations for the eigenenergies are also cumbersome, so we will simply point out the primary effect of interest to us. The electronlike dispersion will have the form

$$E_\pm(k) = a_0 + a_1 k \pm \sqrt{f(k)}, \tag{B15}$$

where $a_0,\, a_1 \in \mathbb{R}$ are constants and $f(k)$ is a second-order polynomial in k. Then the velocities of these modes are

$$\frac{dE_\pm}{dk} = a_1 \pm \frac{1}{2\sqrt{f(k)}}\frac{df}{dk}, \tag{B16}$$

Figure 6 shows the drift velocities calculated directly using Eqs. (B14)–(B16). For the physically relevant regime when $\delta t/t_0 \ll 1$, we see that v_a is quite small and grows linearly with $\delta t/t_0$.

APPENDIX C: TIGHT BINDING MODEL FOR 2DEG-SUPERCONDUCTOR JUNCTION

To estimate the properties of the CAES dispersion, for $\nu = 2$ we use the following tight-binding Bogoliubov–de Gennes Hamiltonian:

$$H_{\rm BdG} = \sum_i \psi_i^\dagger (4t - \mu_i)\tau_z\sigma_0\psi_i + \sum_{\langle ij\rangle}\psi_i^\dagger\left(-te^{i\phi_{i,j}}\frac{\tau_0+\tau_z}{2} + te^{-i\phi_{i,j}}\frac{\tau_0-\tau_z}{2}\right)\sigma_0\psi_j + \frac{\Delta_Z}{2}\sum_i \psi_i^\dagger\tau_0\sigma_z\psi_i + \sum_i \psi_i^\dagger(-\Delta_i\tau_x)\psi_i, \tag{C1}$$

where $\psi_i = (c_{i,\uparrow},\, c_{i,\downarrow},\, c^\dagger_{i,\downarrow},\, -c^\dagger_{i,\uparrow})^T$, $c^\dagger_{i,\sigma}$ $(c_{i,\sigma})$ is the creation (annihilation) operator for an electron at site i with spin σ, τ_i are 2×2 Pauli matrices in particle-hole space, μ_i and Δ_i are the chemical potential and superconducting gap at site i, respectively, and $\phi_{i,j}$ is the Peierls phase introduced to take into account the presence of the magnetic field in the 2DEG. We assume $\Delta_i = \tilde{\Delta}$ in the SC and $\Delta_i = 0$ in the 2DEG. In the 2DEG, μ_i is set to a value $\mu = \hbar\omega_c$ (between the first and second Landau levels). We take the hopping parameter $t = 1.323\,\mathrm{eV}$ and lattice spacing $a = 2.0$ nm to model a quadratic dispersion with effective mass $m^* = 0.1m_e$. We set $\tilde{\Delta} = 1\,\mathrm{meV}$ and consider lead widths $L_x^{(n)} = 200$ nm and $L_x^{(n)} = 600$ nm for the normal and superconductor leads, respectively. In the SC, $\mu_i = \mu_s$, and, in general $\mu_s \neq \mu$. The magnetic field is in the direction z, perpendicular to the xy plane to which the 2DEG is confined: $\mathbf{B} = B\hat{z}$. Using the Landau gauge $\mathbf{A} = Bx\hat{e}_y$ (assuming translational invariance of the leads in the y direction), the Peierls phase is given by the expression

$$\phi_{i,j} = -\frac{2\pi B}{\phi_0}\frac{(y_i+y_j)(x_j-x_i)}{2}, \tag{C2}$$

where (x_i, y_i) are the coordinates of the ith site and $\phi_0 = h/e$ is the quantum Hall magnetic flux quantum.

APPENDIX D: TIGHT BINDING MODEL FOR GRAPHENE-SUPERCONDUCTOR JUNCTION

We consider a three-terminal graphene device with two QH leads (lead 0 and 1) and a single SC lead. The tight-binding Hamiltonian is given by

$$H = H_0 + H_{\rm sc} + H_Z. \tag{D1}$$

In graphene, each unit cell is formed by two carbon atoms, A and B. Atoms A and B form two triangular lattices. Let A_i, and B_i denote the positions of atoms A and B, and $S_i = A_i, B_i$. With this notation, we can write

$$H_0 = \sum_{\langle S_iS_j\rangle}\psi^\dagger_{S_i}\left(-te^{i\phi_{S_i,S_j}}\frac{\tau_0+\tau_z}{2}\right)\sigma_0\psi_{S_j} + \sum_{\langle S_iS_j\rangle}\psi^\dagger_{S_i}\left(te^{-i\phi_{S_i,S_j}}\frac{\tau_0-\tau_z}{2}\right)\sigma_0\psi_{S_j} - \mu\sum_{S_i}\psi^\dagger_{S_i}\tau_z\sigma_0\psi_{S_i}, \tag{D2}$$

$$H_{\rm sc} = \sum_{S_i}\psi^\dagger_{S_i}(-\Delta\tau_y\sigma_y)\psi_{S_i}, \tag{D3}$$

$$H_Z = \sum_{S_i}\psi^\dagger_{S_i}\left(\frac{\Delta_Z}{2}\tau_z\sigma_z\right)\psi_{S_i}, \tag{D4}$$

where $\psi_{S_i} = (c_{S_i,\uparrow},\, c_{S_i,\downarrow},\, c^\dagger_{S_i,\uparrow},\, c^\dagger_{S_i,\downarrow})$, $c^\dagger_{S_i,\sigma}$ $(c^\dagger_{S_i,\sigma})$ is the creation (annihilation) operator for an electron with spin $\sigma = \uparrow, \downarrow$

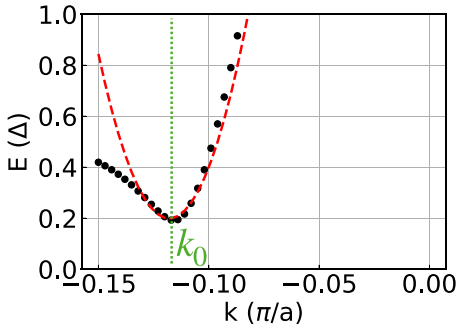

FIG. 7. Left: Parabolic fit (red dashed line) of $\nu = 0$ CAF states (black dots) for $\theta = \pi/4$ generated from the GS tight binding model using parameters used in Fig. 3 of the main text.

at site S_i, $t = 2.8\,\text{eV}$ [27], τ_i and σ_i are Pauli matrices in Nambu and spin space, respectively, μ is the chemical potential with respect to the charge neutrality point and ϕ_{S_i,S_j} is the Peierls phase. Using the same gauge as discussed in the previous section, we have

$$\phi_{S_i,S_j} = -\frac{2\pi B}{\phi_0}\frac{\left(S_{i_y}+S_{j_y}\right)\left(S_{j_x}-S_{i_x}\right)}{2}, \tag{D5}$$

where (S_{i_x}, S_{j_y}) are the coordinates of site S_i. The magnetic field used in our simulations is $B = 200\,\text{T}$, which is artificially large to compensate for a small scattering region, giving us a magnetic flux comparable to experiment ($\Phi_{tot}/\Phi_0 \approx 345$) and to fix the ratio $l_B/\xi_{sc} = 0.175$ and $L_{sc}/\xi = 0.675$.

We use this tight-binding model as the basis for the fit of $\nu = 0$ states in the CAF phase. In Fig. 7, we show the fit for $\theta = \pi/4$ used to generate Fig. 4 in the main text and confirm that the nanowire model for the $k_0 = 0$ case hosts Majorana zero modes at the ends.

APPENDIX E: CALCULATION OF TRANSPORT PROPERTIES

After implementing the tight-binding model via the Python package KWANT [53], we obtain the local and nonlocal conductances transmission probabilities $T^{pe}_{j,0} = \sum_n^{N_{mode}} t^{pe}_{j,0}(n)$ where $t^{pe}_{j,0}(n)$ is the probability of an incident electron from the nth band of lead 0 to be scattered to lead j as an electron or hole (p = e,h). The nonlocal downstream conductance is

$$G_D = \sum_n^{N_{modes}} \left(T^{e\text{-}e}_{1,0}(n) - T^{h\text{-}e}_{1,0}(n)\right) \tag{E1}$$

and the nonlocal Andreev conductance is

$$G_{AR} = \sum_n^{N_{modes}} \left(T^{he}_{0,0}(n) - T^{he}_{1,0}(n)\right). \tag{E2}$$

The upstream and downstream resistances are calculated using a Landauer-Büttiker approach and found to be [21]

$$R_U = \frac{R_H}{\nu}\left(\frac{2T^{h\text{-}e}_{1,0} + T^{h\text{-}e}_{0,1} + T^{e\text{-}e}_{0,1}}{2D}\right) \tag{E3}$$

$$R_D = \frac{R_H}{\nu}\left(\frac{T^{e\text{-}e}_{1,0} - T^{h\text{-}e}_{1,0}}{2D}\right), \tag{E4}$$

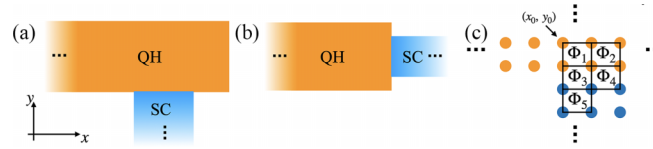

FIG. 8. (a), (b) Two distinct geometries of a NS junction where the two-terminal conductance is expected to be the same for both geometries in the ideal situation. (c) Schematic of the tight-binding lattice at the NS interface.

where

$$D = T^{h\text{-}e}_{0,1}T^{e\text{-}e}_{1,0} + T^{ee}_{0,1}T^{h\text{-}e}_{1,0} + T^{e\text{-}e}_{0,0}\left(T^{h\text{-}e}_{1,1} + T^{h\text{-}e}_{0,1} + T^{e\text{-}e}_{0,1}\right) + T^{h\text{-}e}_{1,1}\left(T^{h\text{-}e}_{0,0} + T^{h\text{-}e}_{1,0} + T^{e\text{-}e}_{1,0}\right). \tag{E5}$$

APPENDIX F: ON THE PEIERLS SUBSTITUTION IN QH-SC JUNCTION SIMULATIONS

Let us consider the two geometries shown in Figs. 8(a) and 8(b). The magnetic field can be accounted for on a lattice by using the Peierls substitution on the hopping t in tight-binding simulations:

$$\sum_{\langle ij\rangle} \psi_i^\dagger(-t)\psi_i \to \sum_{\langle ij\rangle} \psi_i^\dagger(-te^{i\phi_{i,j}})\psi_i, \tag{F1}$$

where $\phi_{i,j}$ is the Peierls phase, Eq. (C2). The Peierls phase, integrated around a plaquette, is the magnetic flux threading the plaquette modulo ϕ_0. We will assume that the S region is in the Meissner phase and take $\vec{A} = 0$. First consider geometry (a) and the flux threading the plaquettes along the NS interface shown in Fig. 8(c). Using $\Phi = \oint d\vec{\ell}\cdot\vec{A}$,

$$\Phi_1 = \Phi_2 = a^2 B, \tag{F2}$$

$$\Phi_3 = \Phi_4 = a(y_0 - a)B, \tag{F3}$$

$$\Phi_5 = 0. \tag{F4}$$

Note that Φ_3, Φ_4 depend on the coordinate system (i.e., y_0). Since Φ is an observable quantity, this cannot be the case. The choice of y_0 is made to smoothly and monotonically take $\Phi \to 0$ across the NS interface. Then we must choose $y_0 \in \{a, 2a\}$. But the reason for the choice of y_0 is even more basic than this. From classic electrostatics, the boundary conditions for the magnetic field imply the vector potential must be continuous across any boundary. Then, since the NS boundary lies between $y \in \{y_0 - a,\ y_0 - 2a\}$, we must have $y_0 \in \{a, 2a\}$ to make $\vec{A}$ continuous across the NS interface.

Turning to geometry (b), we can perform a similar analysis and show that the continuity of $\vec{A}$ along the NS interface is generally *violated*. Hence, we may assume $\vec{A} = 0$ at all S sites *only if* (i) the NS interface is perpendicular to the translationally invariant normal leads and (ii) the coordinate system is chosen such that $\vec{A}$ in the normal region goes to zero at the NS interface.

[1] L. Fu and C. L. Kane, Phys. Rev. Lett. **100**, 096407 (2008).
[2] R. S. K. Mong, D. J. Clarke, J. Alicea, N. H. Lindner, P. Fendley, C. Nayak, Y. Oreg, A. Stern, E. Berg, K. Shtengel, and M. P. A. Fisher, Phys. Rev. X **4**, 011036 (2014).
[3] F. Finocchiaro, F. Guinea, and P. San-Jose, Phys. Rev. Lett. **120**, 116801 (2018).
[4] P. San-Jose, J. L. Lado, R. Aguado, F. Guinea, and J. Fernández-Rossier, Phys. Rev. X **5**, 041042 (2015).
[5] A. Y. Kitaev, Phys. Usp. **44**, 131 (2001).
[6] D. J. Clarke, J. Alicea, and K. Shtengel, Nat. Commun. **4**, 1348 (2013).
[7] P. Rickhaus, M. Weiss, L. Marot, and C. Schönenberger, Nano Lett. **12**, 1942 (2012).
[8] F. Amet, C. T. Ke, I. V. Borzenets, J. Wang, K. Watanabe, T. Taniguchi, R. S. Deacon, M. Yamamoto, Y. Bomze, S. Tarucha, and G. Finkelstein, Science **352**, 966 (2016).
[9] L. Zhao, E. G. Arnault, A. Bondarev, A. Seredinski, T. F. Q. Larson, A. W. Draelos, H. Li, K. Watanabe, T. Taniguchi, F. Amet, H. U. Baranger, and G. Finkelstein, Nat. Phys. **16**, 862 (2020).
[10] G.-H. Lee, K.-F. Huang, D. K. Efetov, D. S. Wei, S. Hart, T. Taniguchi, K. Watanabe, A. Yacoby, and P. Kim, Nat. Phys. **13**, 693 (2017).
[11] O. Gül, Y. Ronen, S. Y. Lee, H. Shapourian, J. Zauberman, Y. H. Lee, K. Watanabe, T. Taniguchi, A. Vishwanath, A. Yacoby, and P. Kim, Phys. Rev. X **12**, 021057 (2022).
[12] M. Hatefipour, J. J. Cuozzo, J. Kanter, W. M. Strickland, C. R. Allemang, T.-M. Lu, E. Rossi, and J. Shabani, Nano Lett. **22**, 6173 (2022).
[13] L. Zhao, Z. Iftikhar, T. F. Q. Larson, E. G. Arnault, K. Watanabe, T. Taniguchi, F. Amet, and G. Finkelstein, Phys. Rev. Lett. **131**, 176604 (2023).
[14] Y. Tang, C. Knapp, and J. Alicea, Phys. Rev. B **106**, 245411 (2022).
[15] A. David, J. S. Meyer, and M. Houzet, Phys. Rev. B **107**, 125416 (2023).
[16] V. D. Kurilovich, Z. M. Raines, and L. I. Glazman, Nat. Commun. **14**, 2237 (2023).
[17] A. B. Michelsen, P. Recher, B. Braunecker, and T. L. Schmidt, Phys. Rev. Res. **5**, 013066 (2023).
[18] V. D. Kurilovich and L. I. Glazman, Phys. Rev. X **13**, 031027 (2023).
[19] A. L. R. Manesco, I. M. Flór, C.-X. Liu, and A. R. Akhmerov, SciPost Phys. Core **5**, 045 (2022).
[20] T. Sekera, C. Bruder, and R. P. Tiwari, Phys. Rev. B **98**, 195418 (2018).
[21] M. Beconcini, M. Polini, and F. Taddei, Phys. Rev. B **97**, 201403(R) (2018).
[22] Z. Hou, Y. Xing, A.-M. Guo, and Q.-F. Sun, Phys. Rev. B **94**, 064516 (2016).
[23] S.-B. Zhang and B. Trauzettel, Phys. Rev. Lett. **122**, 257701 (2019).
[24] Y. Alavirad, J. Lee, Z.-X. Lin, and J. D. Sau, Phys. Rev. B **98**, 214504 (2018).
[25] N. Schiller, B. A. Katzir, A. Stern, E. Berg, N. H. Lindner, and Y. Oreg, Phys. Rev. B **107**, L161105 (2023).
[26] T. H. Galambos, F. Ronetti, B. Hetényi, D. Loss, and J. Klinovaja, Phys. Rev. B **106**, 075410 (2022).
[27] S. Das Sarma, S. Adam, E. H. Hwang, and E. Rossi, Rev. Mod. Phys. **83**, 407 (2011).
[28] M. O. Goerbig, Rev. Mod. Phys. **83**, 1193 (2011).
[29] D. P. Arovas, A. Karlhede, and D. Lilliehöök, Phys. Rev. B **59**, 13147 (1999).
[30] A. A. Burkov and A. H. MacDonald, Phys. Rev. B **66**, 115320 (2002).
[31] Z. F. Ezawa and K. Hasebe, Phys. Rev. B **65**, 075311 (2002).
[32] K. Nomura and A. H. MacDonald, Phys. Rev. Lett. **96**, 256602 (2006).
[33] K. Yang, S. Das Sarma, and A. H. MacDonald, Phys. Rev. B **74**, 075423 (2006).
[34] J. Jung and A. H. MacDonald, Phys. Rev. B **80**, 235417 (2009).
[35] D. A. Abanin, B. E. Feldman, A. Yacoby, and B. I. Halperin, Phys. Rev. B **88**, 115407 (2013).
[36] A. F. Young, C. R. Dean, L. Wang, H. Ren, P. Cadden-Zimansky, K. Watanabe, T. Taniguchi, J. Hone, K. L. Shepard, and P. Kim, Nat. Phys. **8**, 550 (2012).
[37] M. Kharitonov, Phys. Rev. B **85**, 155439 (2012).
[38] A. F. Young, J. D. Sanchez-Yamagishi, B. Hunt, S. H. Choi, K. Watanabe, T. Taniguchi, R. C. Ashoori, and P. Jarillo-Herrero, Nature (London) **505**, 528 (2014).
[39] S. Takei, A. Yacoby, B. I. Halperin, and Y. Tserkovnyak, Phys. Rev. Lett. **116**, 216801 (2016).
[40] D. S. Wei, T. van der Sar, S. H. Lee, K. Watanabe, T. Taniguchi, B. I. Halperin, and A. Yacoby, Science **362**, 229 (2018).
[41] P. Stepanov, S. Che, D. Shcherbakov, J. Yang, R. Chen, K. Thilahar, G. Voigt, M. W. Bockrath, D. Smirnov, K. Watanabe, T. Taniguchi, R. K. Lake, Y. Barlas, A. H. MacDonald, and C. N. Lau, Nat. Phys. **14**, 907 (2018).
[42] X. Liu, G. Farahi, C.-L. Chiu, Z. Papic, K. Watanabe, T. Taniguchi, M. P. Zaletel, and A. Yazdani, Science **375**, 321 (2022).
[43] A. Coissard, D. Wander, H. Vignaud, A. G. Grushin, C. Repellin, K. Watanabe, T. Taniguchi, F. Gay, C. B. Winkelmann, H. Courtois, H. Sellier, and B. Sacépé, Nature (London) **605**, 51 (2022).
[44] H. Zhou, C. Huang, N. Wei, T. Taniguchi, K. Watanabe, M. P. Zaletel, Z. Papić, A. H. MacDonald, and A. F. Young, Phys. Rev. X **12**, 021060 (2022).
[45] H. Hoppe, U. Zülicke, and G. Schön, Phys. Rev. Lett. **84**, 1804 (2000).
[46] F. Giazotto, M. Governale, U. Zülicke, and F. Beltram, Phys. Rev. B **72**, 054518 (2005).
[47] I. M. Khaymovich, N. M. Chtchelkatchev, I. A. Shereshevskii, and A. S. Mel'nikov, Europhys. Lett. **91**, 17005 (2010).
[48] J. A. M. van Ostaay, A. R. Akhmerov, and C. W. J. Beenakker, Phys. Rev. B **83**, 195441 (2011).
[49] B. Lian, J. Wang, and S.-C. Zhang, Phys. Rev. B **93**, 161401(R) (2016).
[50] L. Brey and H. A. Fertig, Phys. Rev. B **73**, 195408 (2006).
[51] K. Wakabayashi, K.-I. Sasaki, T. Nakanishi, and T. Enoki, Sci. Technol. Adv. Mater. **11**, 054504 (2010).
[52] C. W. J. Beenakker, Phys. Rev. Lett. **112**, 070604 (2014).
[53] C. W. Groth, M. Wimmer, A. R. Akhmerov, and X. Waintal, New J. Phys. **16**, 063065 (2014).

[54] K. Nomura, S. Ryu, and D.-H. Lee, Phys. Rev. Lett. **103**, 216801 (2009).
[55] A. Das, R. K. Kaul, and G. Murthy, Phys. Rev. Lett. **128**, 106803 (2022).
[56] S. J. De, A. Das, S. Rao, R. K. Kaul, and G. Murthy, Phys. Rev. B **107**, 125422 (2023).
[57] A. Knothe and T. Jolicoeur, Phys. Rev. B **92**, 165110 (2015).
[58] T. D. Stanescu, R. M. Lutchyn, and S. Das Sarma, Phys. Rev. B **84**, 144522 (2011).
[59] D. B. Chklovskii, B. I. Shklovskii, and L. I. Glazman, Phys. Rev. B **46**, 4026 (1992).